



OPEN Experimental study on laser cutting process of simulated fast Reactor fuel rods

Tianchi Li¹, Zengliang Mo², Qi Chen¹, Jia Zhou¹, Zhi Cao¹, Jianhua Guo¹, Zhongyuan Yang¹, Chunwei Tang², Hongmei Zhang², Tao Xiao², Wensi Li¹, Yuzhou Ming¹, Fang Liu¹, Taihong Yan¹✉, Gaoyang Mi³ & Weifang Zheng¹✉

The cladding of fast reactor fuel rods, made of stainless steel, presents significant challenges in cutting due to its ductility, which leads to increased tool wear and poor cut quality with traditional mechanical methods. Laser cutting has emerged as a superior alternative, offering non-contact precision, high efficiency, and suitability for radioactive environments. This study systematically investigates the effects of laser cutting parameters—cutting speed, focal position, power, and gas pressure—on the cutting quality of simulated fast reactor fuel rods. The results show that optimal cutting is achieved with a cutting speed of 1 m/min, a focal position between – 20 and – 25 mm, a laser power between 7200 and 9600 W, and a gas pressure of 10 MPa. These parameters provide the best balance between cutting efficiency, surface roughness, and minimal slag formation. This study contributes valuable insights into optimizing laser cutting technology for nuclear fuel rod processing, with potential applications in fuel reprocessing and decommissioning.

Keywords Laser cutting, Fast reactor fuel rod, Stainless steel cladding, Cutting quality, Nuclear fuel processing

Fast reactor technology represents a crucial step in maximizing the efficient utilization of uranium resources. One of its essential processes involves the reprocessing of spent fast reactor fuel^{1–6}, where irradiated fuel is treated to extract and purify unburned uranium and newly formed plutonium for recycling^{7–9}. This ensures effective fuel reutilization. However, a significant difference exists between fast reactors and pressurized water reactors in the fuel rod cutting process. Fuel rods are elongated cylindrical structures, typically 1.5 m to 3 m in length and 10 mm to 15 mm in diameter^{10,11}, encased in stainless steel with an additional 1 mm to 2 mm thick stainless steel wire wrapping. Due to the ductile nature of stainless steel, mechanical cutting methods lead to increased tool wear and reduced clean segment rates^{6,12,13}.

With technological advancements, laser cutting has emerged as a focal point of global research^{14–18}. It offers numerous advantages, including high cutting speeds, minimal secondary waste generation, absence of surface deformation or residual stress, suitability for high-radioactive and difficult-to-access areas via fiber optic delivery, extended tool lifespan through non-contact cutting, and applicability to complex and high-precision tasks^{19–22}.

Laser technology is pivotal for the future of fast reactor fuel rod cutting, with countries like India, the United States, and Japan leading in its development for spent fuel components^{23,24}. India has made significant advancements in laser technology, particularly by developing a laser dismantling system for removing fuel pins from wrappers^{25–27}. This system is part of the cutting-edge efforts at the CORAL (COmpact Reprocessing of Advanced fuels in Lead-shielded) facility in Kalpakkam. Furthermore, India has clearly outlined plans to incorporate a laser cutting system into the Demonstration Fast Reactor Fuel Reprocessing Plant (DFRP), demonstrating the feasibility and advantages of using laser shearing technology in hot cell environments^{28,29}.

While laser technology is widely used internationally for cutting the outer casings of fast reactor assemblies, we believe it also offers distinct advantages and potential for cutting fuel rods. The key benefit of laser shearing for fuel rods is its non-contact nature, which effectively eliminates issues like tool head wear, enhancing both equipment reliability and longevity. Our primary focus is on the quality of laser cutting for fuel rods, including the power required, the effectiveness of the cuts, and whether the presence of winding impacts the process. These questions form the basis of our current research objectives.

¹China Institute of Atomic Energy, P. O. Box 275 (26), Beijing 102413, China. ²GZ Photonics Technology Co., Ltd, Dongguan 523808, China. ³School of Materials Science and Engineering, Huazhong University of Science and Technology, Wuhan 430074, China. ✉email: yanthcn@163.com; zhengwfcn@163.com

The requirements for cutting fast reactor fuel rods include achieving minimal kerf width to maximize fuel recovery, minimizing slag deposition on cut surfaces, and ensuring smoothness for efficient transportation of short segments^{19,30–34}. These challenges underscore the importance of laser cutting processes, which involve intricate interactions among material properties, laser beam characteristics, and cutting auxiliary gases^{35–37}. Parameters such as material type, thickness, surface condition, laser mode, power, cutting speed, assist gas type, pressure, focal position, and nozzle dimensions significantly impact cutting quality^{38–40}.

The cladding and helical wire of the fuel rods are made of stainless steel. In recent years, laser cutting technology for stainless steel has seen notable advancements in both efficiency and quality. Laser cutting has become a crucial tool for processing thick steel plates, particularly for high-strength stainless steel, where it shows significant advantages^{38,41,42}. Research indicates that high-power fiber lasers can cut steel plates with thicknesses ranging from 10 to 60 millimeters without the need for auxiliary blowing. Advances in technology have further optimized the focus settings and laser parameters, improving both cutting quality and efficiency, especially in specialized applications like nuclear decommissioning⁴³. Moreover, precise control of laser power and feed rates has resulted in superior edge quality and lower surface roughness, reducing the need for secondary processing⁴⁴. Overall, laser cutting technology for stainless steel, particularly in thick plate cutting and high-precision applications, is gradually replacing traditional methods, becoming a key technology in industrial processing⁴⁵.

The nuclear fuel within the rods is UO₂ ceramic, and laser cutting technology for ceramics has also made significant progress in recent years, particularly in precision machining and material performance enhancement^{46,47}. Laser-assisted machining (LAM) has been widely applied to ceramics due to its ability to overcome the challenges posed by ceramics' high hardness and brittleness^{48–50}. Recent research has focused on optimizing laser cutting parameters such as laser power, feed rate, and scanning speed to reduce surface roughness and improve processing efficiency. For example, ultrafast laser processing of oxide-oxide (Al₂O₃/Al₂O₃) ceramic composites has enhanced cutting precision by minimizing heat-affected zones and mechanical stress⁵¹. Additionally, the use of high-energy laser beams has enabled the cutting and processing of composite ceramic materials⁵², such as high-entropy ceramics⁵³ like silicon carbide⁵⁰, achieving impressive results.

This study employs a self-developed laser cutting platform to investigate how varying parameters—cutting speed, focal position, power, gas pressure, and assist gas type—affect the cutting performance of simulated fuel rod components. Through methods such as photographic observation, optical microscopy, and roughness measurements, the study analyzes and characterizes cutting outcomes under different conditions to identify optimal process parameters.

Experimental methods and materials

Cutting objects

The fast reactor assembly is comprised of a large stainless steel hexagonal tube that encloses a varying number of aligned, slender fuel rod components. In this laser cutting experiment, the focus is on aligned rows of simulated fast reactor fuel rod components. Each fuel rod is wrapped with a stainless steel wire measuring 1–2 mm in diameter, with an overall diameter of approximately 12 mm. The stainless steel cladding of the fuel rod is about 1 mm thick, and its interior is filled with aluminum oxide ceramic to simulate UO₂ fuel. Figure 1 provides a schematic diagram illustrating the stainless steel assembly and the configuration of the fuel rod components. In this experiment, 304 stainless steel was used as the material for the simulated fuel rods.

Experimental facilities

The experiment utilized a cutting table measuring approximately 3 m in length and 2 m in height, equipped with functions for rotating, cutting, and retracting stainless steel components. The laser cutting head employed can withstand up to 15,000 watts of power and includes capacitive focus positioning capability. The laser system utilized is the YMM-12,000 model, a 12,000-watt laser customized by Guozhi Laser, complete with a water chiller, gas cylinder set, control cabinet, and other necessary components. The primary equipment utilized in the experiment is depicted in Fig. 2.

Analytical method

The analysis and testing in this study encompass three main components. Firstly, photographic and visual inspection is used to evaluate the damage to the fuel rod and its wrapping wire. Secondly, a Vernier caliper is

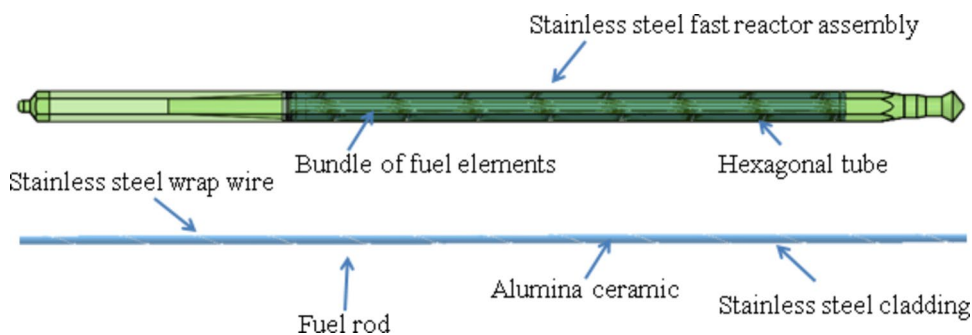


Fig. 1. Schematic diagram of stainless steel component and fuel rod.

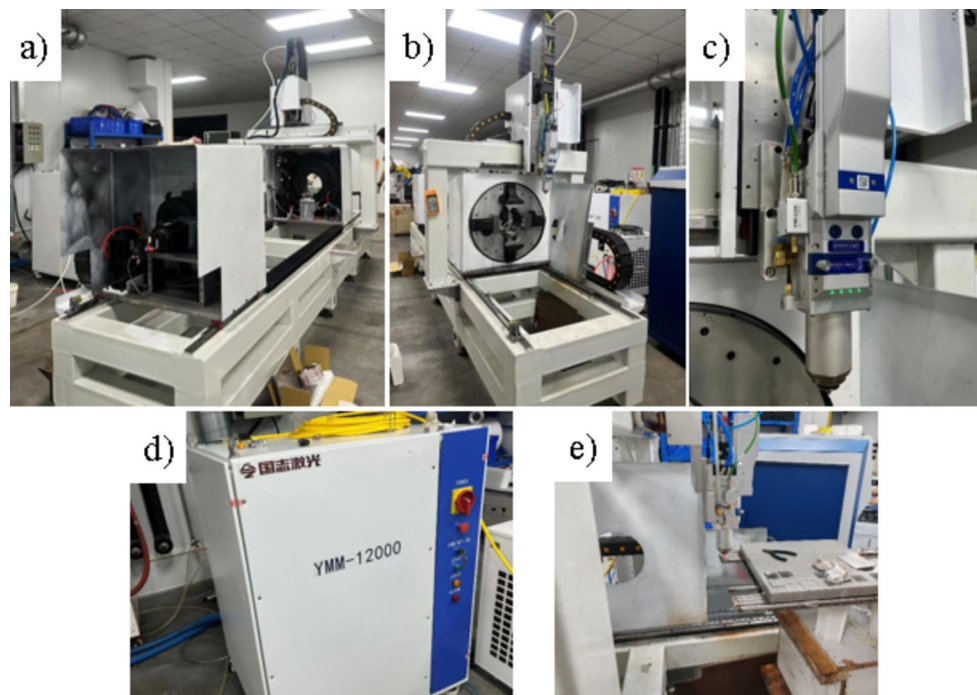


Fig. 2. Main equipment used in the experiment. (a) Rear view of the cutting platform. (b) Front view of the cutting platform. (c) Laser cutting head. (d) Laser generator. (e) Shearing state of aligned fuel rods.

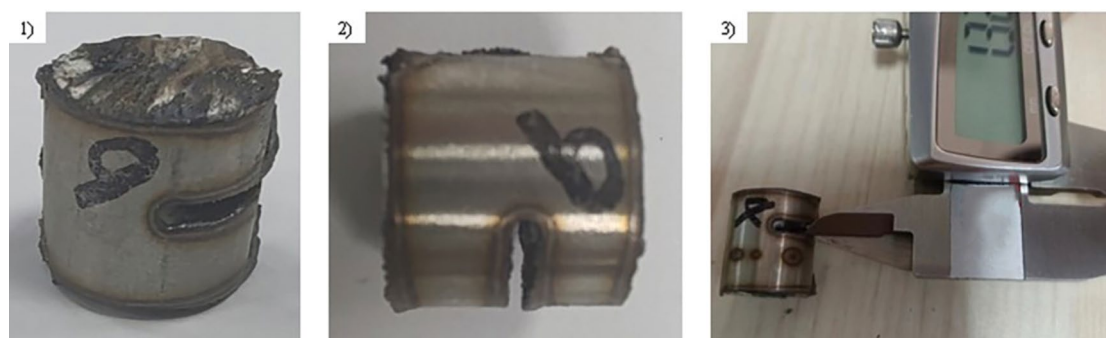


Fig. 3. Schematic diagram of the component to be analyzed.

employed to measure the width of the kerf. Thirdly, an optical microscope is utilized for photography and to measure the length of slag deposits. Additionally, a surface roughness tester is used to quantify the roughness of the cut surfaces.

Optical microscope: Wan Hao Imaging, model VMS-4030.

Surface roughness tester: Wenzhou Jingcheng Measurement Equipment Co., Ltd., model TR100.

Experimental process

The key focus in cutting fuel rod components is on minimizing the width of the kerf, as narrower kerfs result in less damage to the fuel. Attention is also directed towards evaluating the damage to the cut surfaces and the amount of slag deposition. These surfaces will serve as future contact points for dissolution reactions and may affect the transportation of fuel segments. Therefore, before each cutting operation, precise experimental parameters are established and assigned unique experiment numbers. Each experiment involves making two cuts under identical parameters: the first cut slices halfway through a fuel rod component for measuring the kerf width (as shown in Fig. 3), while the second cut completely severs the entire fuel rod for surface characterization (including measuring roughness and inspecting slag deposits under an optical microscope).

The cutting process begins with the cutting head moving laterally across the fuel rod components in the first step, halting upon completion of the cut. In the second step, the cutting head repeats the lateral movement to simultaneously sever all rows of fuel rods and their wrapping wires, as illustrated in Fig. 4.

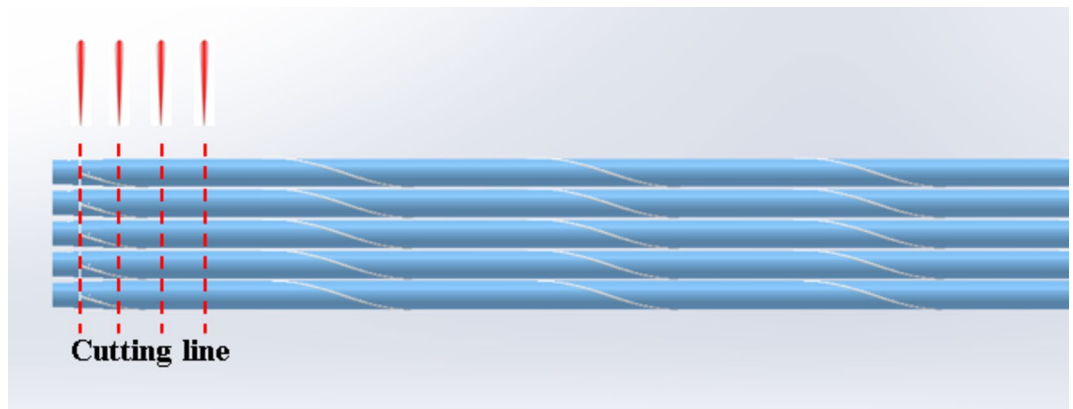


Fig. 4. Laser cutting head movement trajectory.

Fixed parameters	Value
Cutting head lens ratio	1:2
Fiber core diameter (μm)	100
Height of cutting (mm)	10
Diameter of cutting nozzle (mm)	3
Duty ratio (%)	50
Impulse frequency (Hz)	4000

Table 1. Fixed parameters for this experiment.

Experiment parameter

This experiment focuses on examining the impact of cutting speed, focal position, power, type of assist gas, and gas pressure on cutting quality. Parameters such as the ratio of cutting head lenses and fiber core diameter are kept constant throughout. Table 1 lists all the parameters that remain unchanged. These fixed parameters are established based on experience and preliminary tests to identify the optimal settings. Notably, the distance between the cutting nozzle and the component rod is set at 10 mm. This adjustment accounts for the slight lifting of the wire during the cutting process, even with a pressure plate in place. To mitigate any potential interference between the lifted wire and the moving laser cutting head, the nozzle was elevated to 10 mm. Extensive testing has confirmed that at this height, the slightly lifted wire does not affect the movement of the laser cutting head in any way. The experiment's identification number and parameters can be found in Fig. 2. It is important to note that the air used passes through a high-precision filter and a refrigerant dryer. The high-precision filter is designed to achieve a dust content of $0.01 \mu\text{m}$ and an oil content of less than 0.001 ppm. Additionally, the refrigerant dryer maintains a pressure dew point ranging from 3 to 10°C . The parameters of the laser are shown in Table 2.

Results and discussion

In this experiment, rows of components were cut using various cutting parameters, followed by photographing and observing the resulting damage. The observed damage primarily includes cutting marks and the condition of the cross-section on both the fuel rod components and the stainless steel wire wraps. Table 3 details the specific parameters used for each experiment, such as cutting speed, focal position, power, type of assist gas, and gas pressure.

Figure 5 shows the cross-sectional views of laser cuts using two different assist gases: (a) air and (b) nitrogen. From a scientific perspective, the choice of assist gas plays a critical role in the quality and precision of laser cutting.

In the case of air as an assist gas (a), the cutting surface appears rougher with more evident thermal damage and oxidation. This can be attributed to the presence of oxygen in air, which promotes combustion and leads to the formation of oxides on the cut surface, degrading the overall cut quality. Oxidation not only increases surface roughness but also potentially weakens the mechanical properties of the cut edges. In contrast, the nitrogen-assisted cut (b) exhibits a cleaner surface with less thermal damage. Nitrogen, being an inert gas, prevents oxidation and results in a smoother cut edge. This is particularly advantageous for aluminum oxide ceramic, where oxidation-free cuts are often desired for both aesthetic and structural reasons. The reduced presence of oxides and smoother edges in the nitrogen cut make it a more suitable option for high-precision applications requiring minimal post-processing.

Functional parameter	Value	Testing environment
Output rating (W)	12,000 W	Rated power out of light
Polarization direction	Random polarization	–
Controlling power range (%)	10–100%	–
Central wavelength (nm)	1080 ± 10 nm	Rated power out of light
Output power instability (%)	≤ ± 2%	1000 h continuous operation; The operating temperature is 25 °C
Modulation frequency (KHz)	50 KHz	Rated power out of light
Optical quality (BPP, mm-mrad)	<4 mm-mrad (Output path 100 μm)	Rated power out of light
NA	< 0.1	Rated power out of light
Fiber core diameter (μm)	100 μm	–
Output fiber length (m)	20 m	–
External dimension (L×W×H, mm)	1006×918× 1356 mm	–
Weight (kg)	500 kg	–
Working environment temperature range (°C)	10–40 °C	–
Working environment humidity range (%)	< 85%	–

Table 2. Laser parameter.

Experiment numbers	Cutting speed(m/min)	Focal position (mm)	Power(W)	Gaseous medium	Gas pressure(Mpa)
1	0.7	– 20	9600	Air	15
2	1	– 20	9600	Air	15
3	0.3	– 20	9600	Air	15
4	0.7	– 25	9600	Air	15
5	0.7	– 15	9600	Air	15
6	0.7	– 20	12,000	Air	15
7	0.7	– 20	7200	Air	15
8	0.7	– 20	9600	Air	18
9	0.7	– 20	9600	Air	10
10	0.7	– 20	9600	Nitrogen	15
11	1	– 20	9600	Nitrogen	15
12	0.3	– 20	9600	Nitrogen	15
13	0.7	– 25	9600	Nitrogen	15
14	0.7	– 15	9600	Nitrogen	15
15	0.7	– 20	12,000	Nitrogen	15
16	0.7	– 20	7200	Nitrogen	15
17	0.7	– 20	9600	Nitrogen	18
18	0.7	– 20	9600	Nitrogen	10

Table 3. Experiment numbers and parameters for this experiment.

Figure 6 presents the kerf width variations under different cutting parameters—cutting speed, focal position, laser power, and gas pressure. Each parameter has a significant impact on the kerf width, and the observed trends provide insights into the cutting process.

At lower speeds (e.g., 0.3 m/min), the laser has a longer interaction time with the material, resulting in greater heat input and wider kerfs due to excessive melting. As the cutting speed increases (e.g., 1 m/min), the interaction time decreases, reducing heat input and material melting, leading to narrower kerfs. However, excessively high speeds may cause incomplete cuts as the laser energy may not sufficiently penetrate the material. A balance is achieved at moderate speeds, where sufficient energy is delivered without causing excessive material removal. The focal position affects how the laser energy is distributed within the material. A deeper focal position (e.g., – 25 mm) focuses energy more precisely within the material, resulting in narrower kerfs. However, if the focal point is too deep, it may lead to uneven cuts due to insufficient energy near the surface. Shallower focal positions (e.g., – 15 mm) spread the laser energy more across the surface, causing more material to melt and increasing the kerf width. The optimal range, as shown in the results, is between – 20 mm and – 25 mm, where the balance between depth and surface energy leads to the cleanest cuts. Higher laser power (e.g., 12,000 W) delivers more energy, which increases the kerf width by causing excessive material melting. Lower power (e.g., 7200 W) results in narrower kerfs, as less energy is absorbed by the material, preventing unnecessary melting beyond the cut line. However, if the power is too low, it may not fully penetrate the material, leading to incomplete cuts. The

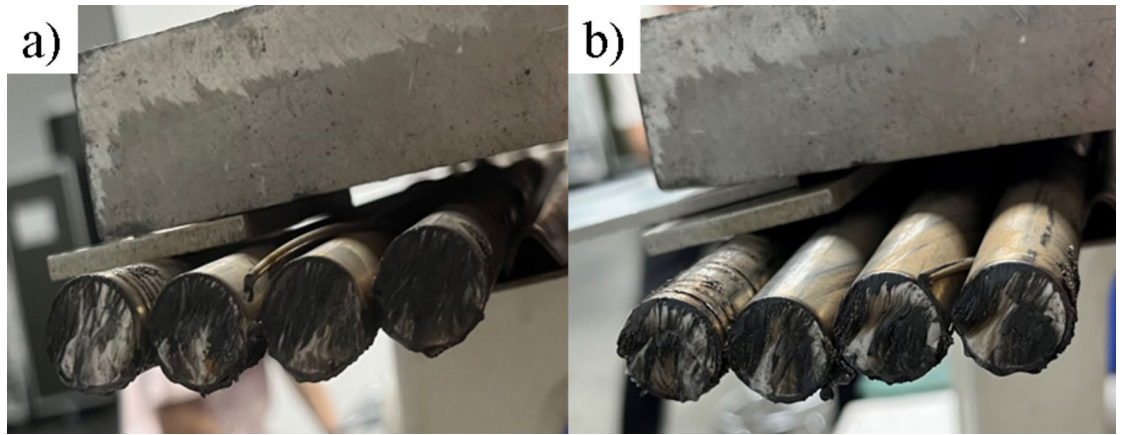


Fig. 5. Cutting results under different gaseous medium (a) air (b) nitrogen.

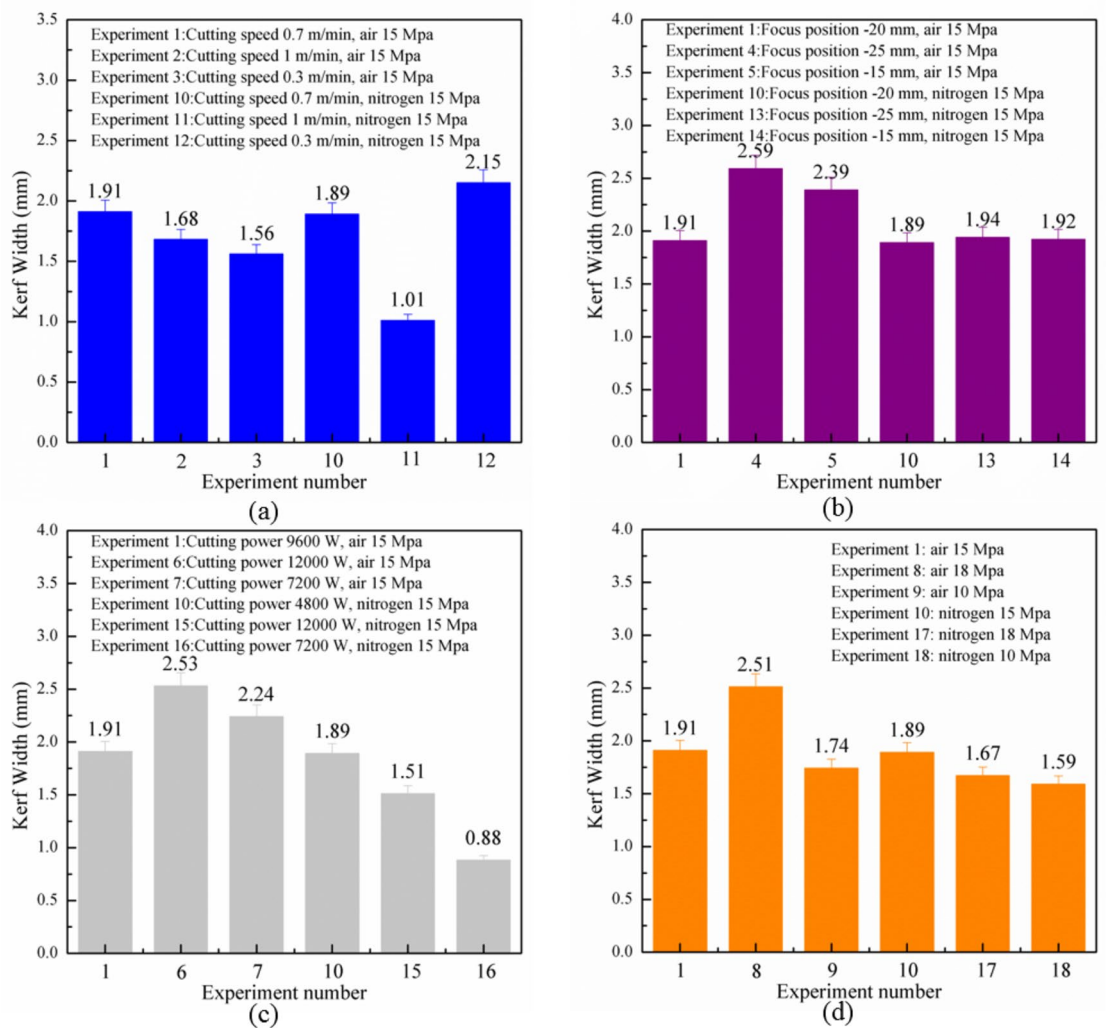


Fig. 6. Kerf width under different cutting parameters (a) Kerf width at different cutting speeds. (b) Kerf width at different focal positions. (c) Kerf width at different powers. (d) Kerf width at different air pressures.

optimal power range (7200 W to 9600 W) achieves a balance by providing enough energy for clean cuts without excessive melting. Gas pressure aids in removing molten material and preventing oxidation. Higher pressures (e.g., 18 MPa with air) can cause turbulence in the cutting zone, leading to wider kerfs due to irregular material ejection. Lower pressures (e.g., 10 MPa) produce more controlled cuts with narrower kerfs. Nitrogen as the assist gas produces less oxidation and narrower kerfs compared to air, and is less sensitive to pressure variations. This makes nitrogen more effective for maintaining precise cuts.

The kerf width is influenced by the balance of laser parameters. Higher cutting speeds, deeper focal positions, and moderate power settings result in narrower kerfs and better precision, while lower speeds, shallow focal positions, and higher power increase the kerf width due to excessive material melting. Gas pressure and type, particularly the use of nitrogen, also contribute to more controlled cuts and narrower kerfs. These observations highlight the importance of optimizing these parameters for efficient and precise laser cutting.

Figure 7 illustrates the surface roughness variations under different cutting parameters, including cutting speed, focal position, laser power, and gas pressure. These parameters directly influence the smoothness of the cut surfaces, and understanding their effects is key to optimizing laser cutting performance.

The results show that lower cutting speeds (e.g., 0.3 m/min) lead to higher surface roughness due to prolonged heat exposure, which causes excessive material melting and rougher edges. Slower speeds result in larger heat-affected zones and material deformation, leading to rougher surfaces. In contrast, higher speeds (e.g., 1 m/min) minimize heat accumulation, creating smoother cuts. However, if the speed is too high, it may lead to incomplete cuts or inconsistent surface quality due to insufficient energy input. Therefore, a moderate cutting speed strikes the best balance between minimizing roughness and ensuring clean cuts. The focal position significantly impacts surface roughness. A deeper focal position (e.g., -25 mm) concentrates energy more effectively within the material, reducing surface roughness as the laser focuses precisely on the cut zone. Deeper focal positions also minimize the heat spread across the surface, resulting in cleaner cuts. Shallower focal positions (e.g., -15 mm)

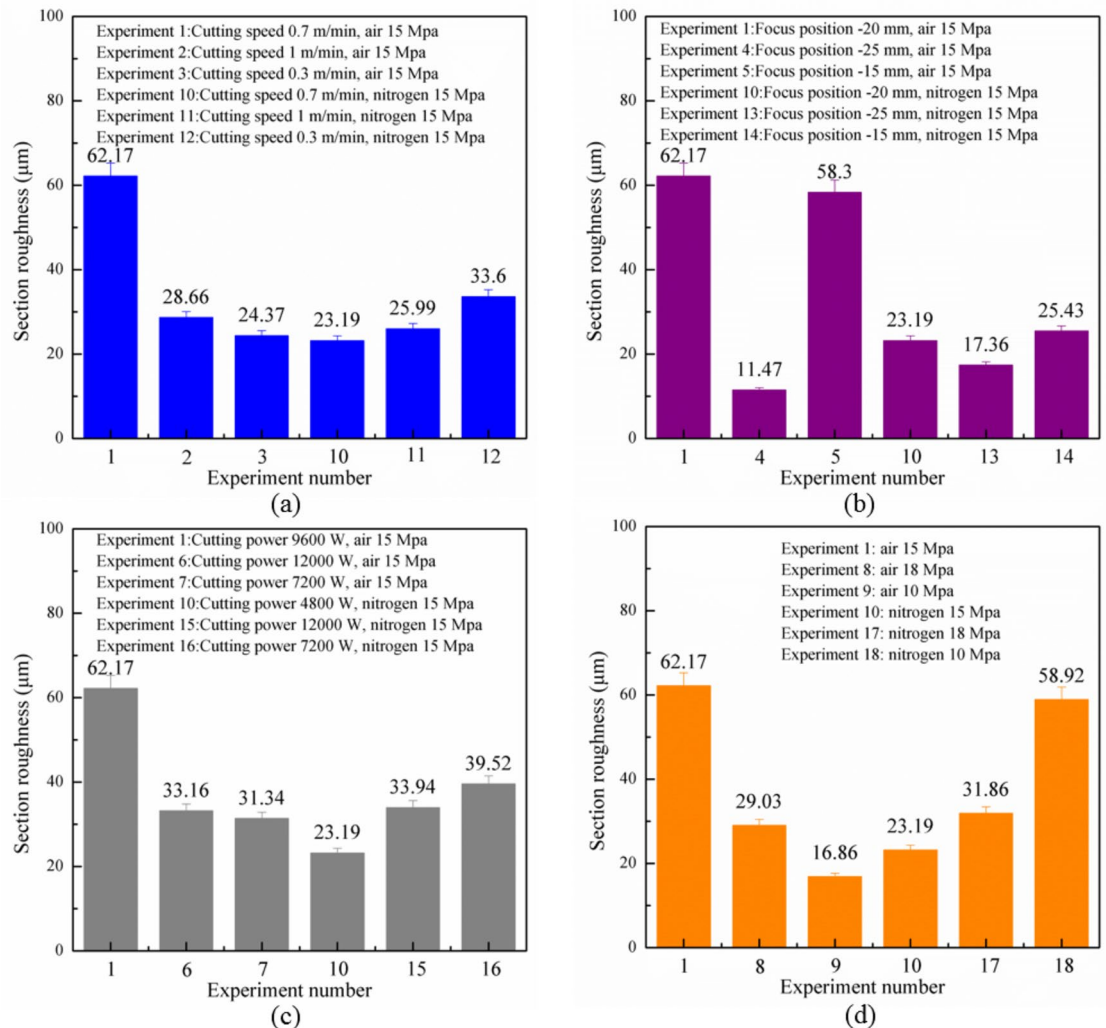


Fig. 7. Surface roughness under different cutting parameters. (a) Roughness at different cutting speeds. (b) Roughness at different focal positions. (c) Roughness at different powers. (d) Roughness at different air pressures.

disperse the laser energy over a broader area, increasing surface roughness due to uneven energy distribution and higher heat input near the surface. The results indicate that a focal position between -20 mm and -25 mm produces the smoothest surfaces. Laser power plays a critical role in determining surface quality. Higher power (e.g., 12000 W) increases surface roughness due to excessive melting, which creates a rougher cut surface as more material is vaporized or left unevenly cooled. Lower power (e.g., 7200 W) produces smoother cuts as less energy is absorbed, resulting in a smaller heat-affected zone and less material melting. However, too little power may lead to incomplete cuts or inconsistent quality. The optimal power range (7200 W to 9600 W) provides sufficient energy to make clean, smooth cuts while minimizing surface roughness. The gas pressure influences the removal of molten material and surface oxidation. Higher pressures (e.g., 18 MPa) are effective in removing molten material from the cut zone, which can reduce surface roughness by preventing slag buildup. However, excessive pressure can lead to turbulence, causing surface irregularities and increasing roughness. Lower pressures (e.g., 10 MPa) result in smoother surfaces, as the gas flow is more controlled and minimizes slag formation. Nitrogen, being an inert gas, further reduces oxidation and promotes smoother cuts compared to air, as evidenced by the experiments using nitrogen at various pressures.

The surface roughness observed in Fig. 7 is primarily influenced by the interaction between the laser and material. Slower speeds, shallow focal positions, and higher power levels increase surface roughness due to excessive heat input and material melting. In contrast, higher speeds, deeper focal positions, and moderate power settings improve surface quality by minimizing heat effects. The choice of assist gas and its pressure also significantly affects the surface finish, with nitrogen and controlled gas pressures producing the smoothest cuts. Optimizing these parameters is essential for achieving the best surface quality in laser cutting processes.

Figure 8 provides magnified cross-sectional images of fuel rods cut under different experimental conditions, revealing variations in cut quality, surface roughness, and slag deposition. These differences can be attributed to key laser cutting parameters such as cutting speed, focal position, laser power, and gas pressure. Below, we discuss the reasons behind these experimental phenomena and the observed data.

The influence of cutting speed is evident in the surface roughness and slag formation. Lower cutting speeds (e.g., Experiment 3) lead to excessive heat accumulation due to prolonged laser-material interaction. This results in greater material melting and significant slag deposition, as well as increased surface roughness. Conversely, higher cutting speeds (e.g., Experiment 2) reduce the interaction time, minimizing thermal effects and producing cleaner cuts with less slag. However, excessively high cutting speeds can compromise cut depth and quality, as the laser energy may not sufficiently penetrate the material. This trade-off highlights the importance of selecting an optimal speed that balances clean cuts with efficient material removal.

Focal position significantly impacts the concentration of laser energy on the material surface and depth. Deeper focal positions (e.g., Experiment 4, -25 mm) concentrate the laser energy within the material, improving cutting precision and reducing kerf width. However, these deeper positions may also lead to excessive material melting and increased slag formation if not well-controlled. Shallower focal positions (e.g., Experiment 5, -15 mm) disperse the energy more broadly across the surface, resulting in wider kerfs and more superficial cuts. The images in Fig. 8 show that a focal position in the range of -20 mm to -25 mm achieves the best balance, with narrower kerfs and minimal slag formation.

Laser power determines the intensity of the energy delivered to the material. Higher power levels (e.g., Experiment 6, 12,000 W) generate increased heat, enabling faster cutting but also leading to more pronounced slag deposition and rougher cut surfaces. This is because excessive power can cause over-melting of the material, especially when combined with slower speeds. On the other hand, lower power settings (e.g., Experiment 7, 7200 W) result in smoother cuts and less slag but may struggle to penetrate the material effectively, particularly in the presence of the wire wrapping. The data suggest that a moderate laser power between 7200 W and 9600 W offers the optimal balance, providing clean cuts with manageable slag levels.

The assist gas plays a crucial role in removing molten material during the cutting process and preventing oxidation. The images in Fig. 8 indicate that higher gas pressures (e.g., Experiment 8, 18 MPa) facilitate better slag removal but can sometimes lead to surface roughness due to turbulence or improper molten material ejection. Lower pressures (e.g., Experiment 9, 10 MPa) reduce the effectiveness of molten material removal, resulting in more slag buildup on the cut surface. Nitrogen, due to its inert nature, generally produces less oxidation compared to air, which is evident in experiments using nitrogen assist gas (e.g., Experiments 13 and 14). However, the benefits of nitrogen are more pronounced at moderate pressures, where slag removal and cut quality are both improved.

The presence of stainless steel wire wrapping adds complexity to the cutting process by influencing how the laser energy is distributed across the surface. The wire acts as a thermal sink, drawing heat away from the rod and potentially leading to uneven melting along the cut surface. This effect is most notable at lower laser powers or when the focal position is not optimized. In the optimized settings (e.g., focal position of -20 mm to -25 mm,



Fig. 8. Enlarged views of the cross-section under different cutting conditions.

cutting speed of 1 m/min, and power between 7200 W and 9600 W), the wire does not significantly hinder the cutting process, and smooth, consistent cuts are achieved.

Figure 9 shows the length of spatter under different cutting parameters, including cutting speed, focal position, laser power, and gas pressure. The spatter length directly reflects how effectively molten material is removed during cutting and is a key factor in determining cut quality.

The spatter length decreases as cutting speed increases. At lower speeds (e.g., 0.3 m/min), the prolonged interaction between the laser and the material causes excessive melting, leading to larger amounts of molten material being ejected, and thus, longer spatter lengths. Higher speeds (e.g., 1 m/min) reduce this interaction time, resulting in less material melting and shorter spatter lengths. However, if the cutting speed is too high, the laser may not deliver sufficient energy to fully cut through the material, potentially leading to incomplete cuts. The focal position influences spatter length by affecting where the laser energy is concentrated. A deeper focal position (e.g., -25 mm) concentrates energy within the material, reducing spatter as less material is melted on the surface. Shallower focal positions (e.g., -15 mm) disperse the laser energy over a larger surface area, causing more material to melt and leading to longer spatter lengths. The results suggest that deeper focal positions help control spatter formation by focusing energy deeper within the cut. Higher laser power (e.g., 12000 W) leads to increased spatter length due to excessive material melting and vaporization. More molten material is generated, which results in larger amounts of spatter being ejected. Conversely, lower power (e.g., 7200 W) generates less heat, reducing material melting and, therefore, shortening the spatter length. A moderate power setting (e.g., 9600 W) provides a balance between cutting efficiency and minimizing spatter. Higher laser power (e.g., 12000 W) leads to increased spatter length due to excessive material melting and vaporization. More molten material is generated, which results in larger amounts of spatter being ejected. Conversely, lower power (e.g.,

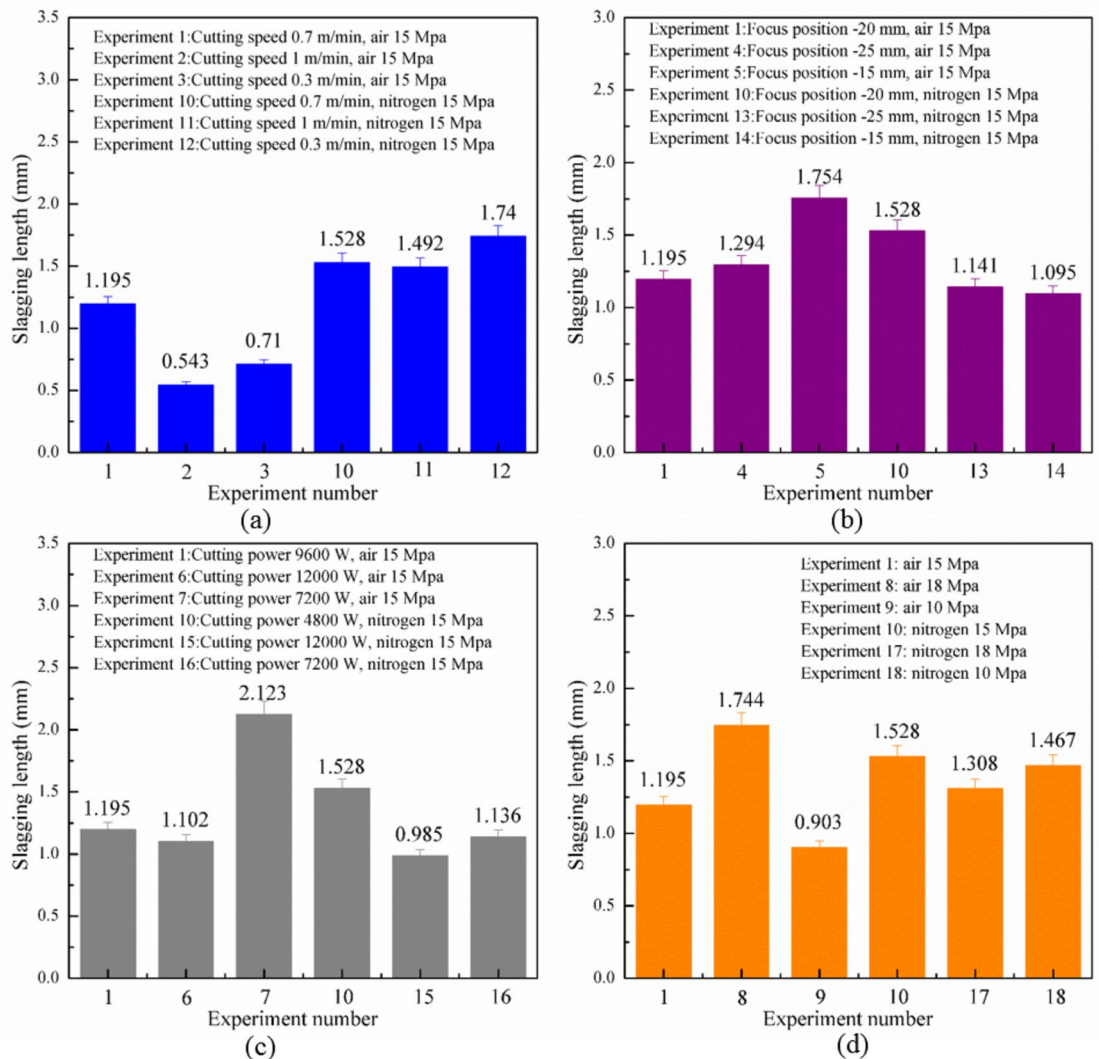


Fig. 9. Length of spatter under different cutting parameters. (a) Length of spatter at different cutting speeds. (b) Length of spatter at different focal positions. (c) Length of spatter at different powers. (d) Length of spatter at different air pressures.

7200 W) generates less heat, reducing material melting and, therefore, shortening the spatter length. A moderate power setting (e.g., 9600 W) provides a balance between cutting efficiency and minimizing spatter.

The spatter length is influenced by the balance of laser parameters. Higher speeds, deeper focal positions, moderate power, and controlled gas pressures contribute to shorter spatter lengths, while lower speeds, shallow focal positions, and higher power increase spatter due to excessive material melting. Optimizing these parameters is crucial for minimizing spatter and achieving cleaner cuts.

Conclusion and future scope

This study systematically investigated the influence of key laser cutting parameters—including cutting speed, focal position, laser power, and gas pressure—on the cutting quality of simulated fast reactor fuel rod bundles. Through a series of controlled experiments, we identified optimal settings that balance cutting efficiency and quality, offering valuable insights into the application of laser cutting for nuclear fuel rod processing. The main conclusions drawn from this study are as follows:

- (1) This study successfully achieved the laser cutting of 1:1 scale simulated fuel rods with wire wrapping using a high-power laser system. The rods were cleanly cut, and the presence of the wire wrapping did not interfere with the movement of the laser cutting head.
- (2) A speed of 1 m/min achieved the best balance between cutting precision and efficiency, minimizing roughness and slag formation. Focal positions between -20 mm and -25 mm provided optimal kerf width and minimal slag, concentrating energy at the best point for precise cutting. A power range of 7200 W to 9600 W delivered the best cutting quality, minimizing surface defects, while excessive power led to rougher cuts. A gas pressure of 10 MPa with air gave the most consistent results for slag removal and clean cuts. Nitrogen performed well but was less sensitive to pressure changes.

Future scope

As the demand for efficient and precise fuel rod cutting increases in nuclear energy applications, laser cutting technology will continue to evolve. Future research should focus on the following areas.

- (1) **Advancements in Laser Technology:** As ultrafast laser systems and higher-power fiber lasers become more accessible, future studies should investigate their potential to further enhance cutting precision and reduce the need for post-processing. Additionally, intelligent control systems could enable real-time adjustments to cutting parameters for even more precise results.
- (2) **Remote Operation in Radioactive Environments:** The non-contact nature of laser cutting makes it ideal for applications in highly radioactive environments, such as nuclear decommissioning and fuel reprocessing facilities. Future research should focus on improving the reliability and safety of remote-operated laser cutting systems in these hazardous settings, where manual intervention is not feasible.
- (3) **Integration of Automation:** Automation of laser cutting processes can further improve operational efficiency and safety, particularly in environments where human exposure is risky. Developing fully automated systems for cutting and handling nuclear fuel rods will be critical for scaling up this technology in practical applications.
- (4) **Material-Specific Optimization:** In this study, aluminum oxide ceramic was used as a simulation of nuclear fuel. However, actual spent fuel contains hundreds of elements, and it is essential to first understand the effects of the laser on key elements such as uranium (U) and plutonium (Pu) before confirming its suitability for cutting fuel rods. So far, we have conducted preliminary cutting tests on UO_2 and found that the laser process does not affect its dissolution in nitric acid⁵⁴. Moving forward, we will continue to explore the interactions between various elements and the laser, along with their potential impacts.

Data availability

The datasets used and/or analysed during the current study available from the corresponding author on reasonable request.

Received: 7 July 2024; Accepted: 25 November 2024

Published online: 27 November 2024

References

1. Wang, M. et al. The role of advanced reactors technologies in China in achieving carbon neutral goals. In *Proceedings of the International Conference on Nuclear Engineering (ICONE) 1933–1940* (2023).
2. Ochoa, R., Jimenez, G. & Perez-Martin, S. Analysis of a Spanish energy scenario with Generation IV nuclear reactors. *Energy Convers. Manag.* **75**, 389–397. <https://doi.org/10.1016/j.enconman.2013.06.038> (2013).
3. Zou, J., Zhao, J., Gudowski, W. & Chmielarz, B. Study of minor actinides transmutation in a lead-cooled fast reactor. In *Proceedings of the International Conference on Nuclear Engineering (ICONE) 1479–1491* (2019).
4. Banerjee, S. & Gupta, H. The evolution of the Indian nuclear power programme. *Prog Nucl. Energy* **101**, 4–18. <https://doi.org/10.1016/j.pnucene.2017.02.008> (2017).
5. Niwa, H., Aoto, K. & Morishita, M. *Current Status and Perspective of Advanced Loop Type Fast Reactor in Fast Reactor Cycle Technology Development Project* (American Nuclear Society, 2007).
6. Li, T. et al. Dissolution of mixed oxide (MOX) fuel in nitric acid: a review. *Heliyon* **10**(6), E27502. <https://doi.org/10.1016/j.heliyon.2024.e27502> (2024).
7. Ion, S. Reaction: recycling and generation IV systems. *Chemistry* **1**(5), 663–665. <https://doi.org/10.1016/j.chempr.2016.10.008> (2016).
8. Adamov, E. et al. Spent nuclear fuel reprocessing and nuclear materials recycling in two-component nuclear energy. *Atom. Energy* **130**(1), 29–35. <https://doi.org/10.1007/s10512-021-00769-w> (2021).

9. Xian, L., Tian, G., Beavers, C. M., Teat, S. J. & Shuh, D. K. Glutarimidedioxime: a complexing and reducing reagent for plutonium recovery from spent nuclear fuel reprocessing. *Angew. Chem. Int. Ed. Engl.* **55**(15), 4671–4673. <https://doi.org/10.1002/anie.201510712> (2016).
10. Ren, F. Y. & Zhou, Z. X. *Foreign Nuclear Fuel Reprocessing* (Atomic Energy, 2006).
11. Zhang, Z. F., Wang, J. F. & Zhang, T. X. *Power Reactor Nuclear Fuel Reprocessing Technology* (Atomic Energy, 2013).
12. Satish, K. V. et al. Vibration analysis and diagnostics of a high speed centrifuge for fast reactor fuel reprocessing applications. *Int. J. Struct. Stab. Dyn.* **23**(19), 2350184. <https://doi.org/10.1142/S0219455423501845> (2023).
13. He, L. Y. et al. Effect of reprocessing on neutrons of a molten chloride salt fast reactor. *Nucl. Sci. Technol.* **34**(3), 46. <https://doi.org/10.1007/s41365-023-01186-3> (2023).
14. Hidetoshi, H. et al. ICONE19-43720 engineering scale tests of mechanical disassembly and short stroke shearing systems for FBR fuel assembly. In *Proceedings of the International Conference on Nuclear Engineering* 19–35 (2011).
15. Birely, J., Cartwright, D. & Marinuzzi, J. Application of high power lasers to problems in the nuclear fuel cycle. In *Ultra High Power Lasers Pract. Appl.* 124–131 (1976).
16. Kongiang, S., Rojananan, S. & Thipprakmas, S. Cut surface characteristics of aluminum alloy sheet in cryogenic shearing process. *Proc. Inst. Mech. Eng. E J. Process. Mech. Eng.* <https://doi.org/10.1177/09544089231221529> (2024).
17. He, Y. et al. Laser cutting technologies and corresponding pollution control strategy. *Processes* **10**(4), 732. <https://doi.org/10.3390/pr10040732> (2022).
18. Liu, S. et al. A state-of-the-art review of radioactive decontamination technologies: facing the upcoming wave of decommissioning and dismantling of nuclear facilities. *Sustainability* **14**(7), 4021. <https://doi.org/10.3390/su14074021> (2022).
19. Oh, S., Lee, I., Park, Y. B. & Ki, H. Investigation of cut quality in fiber laser cutting of CFRP. *Opt. Laser Technol.* **113**, 129–140. <https://doi.org/10.1016/j.optlastec.2018.12.018> (2019).
20. Dodds, J. M. & Rawcliffe, J. Radionuclide distribution during ytterbium doped fibre laser cutting for nuclear decommissioning. *Prog. Nucl. Energy.* **118**, 103122. <https://doi.org/10.1016/j.pnucene.2019.103122> (2020).
21. Sharma, A. K. et al. Investigation of aerosol generation through laser cleaning of various surfaces and optimization of mist & spray scavenging. *J. Aerosol Sci.* **177**, 106329. <https://doi.org/10.1016/j.jaerosci.2023.106329> (2024).
22. Takahashi, K., Watanabe, T. & Kurosawa, K. Development of thick plate cutting technology with fiber-delivered high power nd: YAG laser beam. In *Int. Congress Appl. Lasers Electro-Optics* 229–237 (2001).
23. DAGuin, P. et al. LD-SAFE Project: Laser dismantling environmental and safety assessment-laser cutting demonstration for nuclear power reactors dismantling. In *International Conference on Radioactive Waste Management and Environmental Remediation* 1–8 (2023).
24. Shin, J. S. et al. Underwater laser cutting of thick stainless steel in various cutting directions for application to nuclear decommissioning. *J. Nucl. Fuel Cycle Waste Technol.* **19**(3), 279–287. <https://doi.org/10.7733/jnfcwt.2021.19.3.279> (2021).
25. Shadrin, A. Y. et al. Hydrometallurgical reprocessing of BREST-OD-300 mixed uranium-plutonium nuclear fuel. *Procedia Chem.* **21**, 148–155. <https://doi.org/10.1016/j.proche.2016.10.021> (2016).
26. Natarajan, R. Reprocessing of spent fast reactor nuclear fuels. In *Reprocessing and Recycling of Spent Nuclear Fuel* (ed Taylor, R.) 213–243 (Woodhead Publishing, 2015).
27. Natarajan, R. & Raj, B. Fast reactor fuel reprocessing technology in India. *J. Nucl. Sci. Technol.* **44**(3), 393–397 (2007).
28. Natarajan, R., Vijayakumar, V., Subba Rao, R. & Pandey, N. Experiences of reprocessing of plutonium-rich mixed carbide fuels. *J. Radioanal. Nucl. Chem.* **304**, 401–407. <https://doi.org/10.1007/s10967-015-4000-1> (2015).
29. Kodandaraman, J., Ananda, R., Shekhar, K., Pandey, N. & Ravisankar, A. *Concurrent Trends in Indian Fast Reactor Fuel Reprocessing*. <https://media.superevent.com/documents/20170618/5fc8c3ac5400a00ff04af1740d8a2ca/fr17-297.pdf> (2017).
30. Wu, Z. et al. Effect of laser cutting process parameters on the cutting quality of AZ31B magnesium alloy. *J. Mater. Eng. Perform.* **32**(11), 5201–5210. <https://doi.org/10.1007/s11665-022-07459-z> (2023).
31. Liu, Y. & Zhang, S. Improving the cutting process and quality of thick plates with high-power fiber laser. *Opt. Fiber Technol.* **83**, 103684. <https://doi.org/10.1016/j.yofte.2024.103684> (2024).
32. Singh, T., Arab, J. & Chen, S. C. Improvement on surface quality of Inconel-718 slits via laser cutting and wire electrochemical machining processes. *Opt. Laser Technol.* **167**, 109637. <https://doi.org/10.1016/j.optlastec.2023.109637> (2023).
33. Kim, K. et al. Effect of assist gas pressure on cutting quality in underwater cutting of stainless steel using high-power fiber laser. *Mod. Phys. Lett. B* **36**(16), 2242012. <https://doi.org/10.1142/S021798492242012X> (2022).
34. Keles, O. & Yilbas, B. S. Laser cutting of 2024 aluminium alloy and cutting quality assessment. *Adv. Mater. Process. Technol.* **1**(1–2), 164–171. <https://doi.org/10.1080/2374068X.2015.1116284> (2015).
35. Li, M., Han, H., Jiang, X., Zhang, X. & Chen, Y. Surface morphology and defect characterization during high-power fiber laser cutting of SiC particles reinforced aluminum metal matrix composite. *Opt. Laser Technol.* **155**, 108419. <https://doi.org/10.1016/j.optlastec.2022.108419> (2022).
36. Kovalev, O. & Zaitsev, A. Modeling the problems of conjugate heat and mass transfer in processes of gas-laser cutting of materials. *Heat. Transf. Res.* **36**(7), 601–614. <https://doi.org/10.1615/HeatTransRes.v36.i7.60> (2005).
37. Yilbas, B. A role of lasers in energy materials and future perspectives. *Int. J. Energy Res.* **42**(2), 325–328. <https://doi.org/10.1002/er.3857> (2018).
38. Liao, W., Wang, G., Zhong, L., Chen, Y. & Wang, J. Feasibility analysis and cutting process research on laser cutting medium-thick 20CrNiMo steel plates using a high-power fiber laser without assisted blowing. *J. Manuf. Processes* **111**, 130–138. <https://doi.org/10.1016/j.jmapro.2024.01.020> (2024).
39. Kanyilmaz, A. The problematic nature of steel hollow section joint fabrication, and a remedy using laser cutting technology: a review of research, applications, opportunities. *Eng. Struct.* **183**, 1027–1048. <https://doi.org/10.1016/j.engstruct.2018.12.080> (2019).
40. Angelova, Y. P. Factors influencing the laser treatment of textile materials: an overview. *J. Eng. Fibers Fabric.* **15**, 1–16. <https://doi.org/10.1177/1558925020952803> (2020).
41. Safari, M., Abtahi, S. M. & Joudaki, J. Experimental modeling statistical analysis, and optimization of the laser-cutting process of Hardox 400 steel. *Materials* **17**(12), 2798. <https://doi.org/10.3390/ma17122798> (2024).
42. Chen, J., Tu, F., Wang, P. & Cao, Y. Revealing the enhancement mechanism of laser cutting on the strength–ductility combination in low carbon steel. *Metals* **14**(5), 541. <https://doi.org/10.3390/met14050541> (2024).
43. Shin, J. S., Song, K. H., Oh, S. Y. & Park, S. K. Laser cutting studies on 10–60 mm thick stainless steels with a short focus head for nuclear decommissioning. *Opt. Laser Technol.* **169**, 110121. <https://doi.org/10.1016/j.optlastec.2023.110121> (2024).
44. Muralidharan, K. et al. Parametric analysis and performance of laser cutting on strenx steel. *Mater. Today Proc.* **45**, 2313–2316. <https://doi.org/10.1016/j.matpr.2020.10.573> (2021).
45. Mekala, K. et al. Optimization of cylindrical grinding parameters of austenitic stainless steel rods (AISI 316) by Taguchi method. *Int. J. Mech. Eng. Robot. Res.* **3**(2), 208 (2014).
46. Khadivipannah, P., Olivella, S., Pintado, X. & Vaunat, J. Analysis of shear mock-up tests in a canister-clay system for spent nuclear fuel isolation. *Geomech. Energy Environ.* **32**, 100361. <https://doi.org/10.1016/j.gete.2022.100361> (2022).
47. Kalvettukaran, P., Keshari, P. & Misra, D. Parametric study of laser cutting of glazed ceramic tiles. *J. Braz. Soc. Mech. Sci. Eng.* **45**(6), 333. <https://doi.org/10.1007/s40430-023-04247-1> (2023).

48. Evans, J. A., Anderson, S. A., Faierson, E. J., Perez-Nunez, D. & Mcdeavitt, S. M. Anisotropic radiation-induced changes in type 316L stainless steel rods built by laser additive manufacturing. *Nucl. Technol.* **205**(4), 563–581. <https://doi.org/10.1080/00295450.2018.1502001> (2019).
49. Fan, M., Zhou, X. & Song, J. Experimental investigation on cutting force and machining parameters optimization in in-situ laser-assisted machining of glass–ceramic. *Opt. Laser Technol.* **169**, 110109. <https://doi.org/10.1016/j.optlastec.2023.110109> (2024).
50. Cao, C. et al. Experimental study of plastic cutting in laser-assisted machining of SiC ceramics. *Opt. Laser Technol.* **169**, 110098. <https://doi.org/10.1016/j.optlastec.2023.110098> (2024).
51. Radhakrishnan, J. & Marimuthu, S. Machining of Ox–Ox ($\text{Al}_2\text{O}_3/\text{Al}_2\text{O}_3$) ceramics matrix composites by ultrafast laser. *Ceram. Int.* **50**(20), 39678–39686. <https://doi.org/10.1016/j.ceramint.2024.07.347> (2024).
52. Ghosh, P., Nix, J., Elkington, H., Smith, B. & Marimuthu, S. High power laser cutting of SiC– Al_2O_3 ceramic matrix composites. *Procedia CIRP* **123**, 340–345. <https://doi.org/10.1016/j.procir.2024.05.060> (2024).
53. Wang, J. et al. Nanosecond-laser cutting of (TiZrHfNbTa) C high-entropy ceramics. *Ceram. Int.* **50**(16), 29001–29005. <https://doi.org/10.1016/j.ceramint.2024.05.094> (2024).
54. Chang, S. et al. Microstructure and dissolution of UO₂ pellet after cutting by fiber laser. *Opt. Laser Technol.* **132**, 106493. <https://doi.org/10.1016/j.optlastec.2020.106493>

Author contributions

Yuzhou Ming, Fang Liu, Taihong Yan, Gaoyang Mi, Weifang Zheng has carried on the design of experiments-Tianchi Li, Zengliang Mo, Qi Chen, Jia Zhou, Zhi Cao, Jianhua Guo, Zhongyuan Yang, Chunwei Tang, Hongmei Zhang, Tao Xiaoprocedured, assembled, debugged the experimental setup, conducted experiments, and analyzed the data. Tianchi Li, Zengliang Mo, Qi Chen Wrote the initial draft of the manuscript. Wensi Li Scientifically polished the language of the manuscript. Taihong Yan and Weifang Zheng Proofread the final manuscript.

Funding

National Key R&D Program of China (2022YFB4603000).

Declarations

Competing interests

The authors declare no competing interests.

Additional information

Correspondence and requests for materials should be addressed to T.Y. or W.Z.

Reprints and permissions information is available at www.nature.com/reprints.

Publisher's note Springer Nature remains neutral with regard to jurisdictional claims in published maps and institutional affiliations.

Open Access This article is licensed under a Creative Commons Attribution-NonCommercial-NoDerivatives 4.0 International License, which permits any non-commercial use, sharing, distribution and reproduction in any medium or format, as long as you give appropriate credit to the original author(s) and the source, provide a link to the Creative Commons licence, and indicate if you modified the licensed material. You do not have permission under this licence to share adapted material derived from this article or parts of it. The images or other third party material in this article are included in the article's Creative Commons licence, unless indicated otherwise in a credit line to the material. If material is not included in the article's Creative Commons licence and your intended use is not permitted by statutory regulation or exceeds the permitted use, you will need to obtain permission directly from the copyright holder. To view a copy of this licence, visit <http://creativecommons.org/licenses/by-nc-nd/4.0/>.

© The Author(s) 2024